UNIVERSIDADE ESTADUAL PAULISTA
"JÚLIO DE MESQUITA FILHO"

PROGRAMA DE PÓS-GRADUAÇÃO EM CIÊNCIAS BIOMOLECULARES E FARMACOLÓGICAS

(PPG-FARMATEC)

Instituto de Biociências de Botucatu - Unesp

Desenvolvimento e implementação de um sistema tomográfico para a reconstrução quantitativa de micro partículas magnéticas baseado em sensores de Biosusceptometria AC

LAIS PEREIRA BURANELLO

Dissertação de mestrado apresentada ao Instituto de Biociências, Universidade Estadual Paulista "Júlio de Mesquita Filho", Campus de Botucatu, para obtenção do título de Mestre em Ciências Biomoleculares e Farmacológicas.

Orientador: Prof. Titular Dr. José Ricardo de Arruda Miranda

Coorientador: Dr. André Gonçalves Próspero

Botucatu

2022

FICHA CATALOGRAFICA

FICHA CATALOGRÁFICA ELABORADA PELA SEÇÃO TÉC. AQUIS. TRATAMENTO DA INFORM.
DIVISÃO TÉCNICA DE BIBLIOTECA E DOCUMENTAÇÃO - CÂMPUS DE BOTUCATU - UNESP
BIBLIOTECÁRIA RESPONSÁVEL: ROSEMEIRE APARECIDA VICENTE-CRB 8/5651

Buranello, Lais Pereira.
Desenvolvimento e implementação de um sistema tomográfico para a reconstrução quantitativa de micro partículas magnéticas baseado em sensores de Biosusceptometria AC / Lais Pereira Buranello. - Botucatu, 2022

Dissertação (mestrado) - Universidade Estadual Paulista "Júlio de Mesquita Filho", Instituto de Biociências de Botucatu
Orientador: José Ricardo de Arruda Miranda
Coorientador: André Gonçalves Próspero
Capes: 30402000

1. Biosusceptometria de corrente alternada. 2. Materiais magnéticos. 3. Processamento de imagens - Técnicas digitais. 4. Partículas magnéticas.

Palavras-chave: Biosusceptometria de corrente alternada; Imagiamento quantitativo e tomográfico; Micro e nano materiais magnéticos.

UNIVERSIDADE ESTADUAL PAULISTA

Câmpus de Botucatu

ATA DA DEFESA PÚBLICA DA DISSERTAÇÃO DE MESTRADO DE LAÍS PEREIRA BURANELLO, DISCENTE DO PROGRAMA DE PÓS-GRADUAÇÃO EM FARMACOLOGIA E BIOTECNOLOGIA, DO INSTITUTO DE BIOCIÊNCIAS - CÂMPUS DE BOTUCATU.

Aos 22 dias do mês de novembro do ano de 2022, às 14:00 horas, por meio de Videoconferência, realizou-se a defesa de DISSERTAÇÃO DE MESTRADO de LAÍS PEREIRA BURANELLO, intitulada **Desenvolvimento e implementação de um sistema tomográfico para a reconstrução quantitativa de micro particulas magnéticas baseado em sensores de Biosusceptometria AC.**. A Comissão Examinadora foi constituida pelos seguintes membros: Prof. Dr. ANDRE GONÇALVES PROSPERO (Co-orientador(a) - Participação Virtual) do(a) Departamento de Biofisica e Farmacologia / INSTITUTO DE BIOCIÊNCIAS DE BOTUCATU - UNESP, Prof. Assoc. JOEL MESA HORMAZA (Participação Virtual) do(a) Departamento de Biofisica e Farmacologia / Instituto de Biociências de Botucatu - UNESP, Prof. Dr. OSWALDO BAFFA FILHO (Participação Virtual) do(a) Departamento de Física / Faculdade de Filosofia, Ciências e Letras de Ribeirão Preto - FFCLRP - USP. Após a exposição pela mestranda e arguição pelos membros da Comissão Examinadora que participaram do ato, de forma presencial e/ou virtual, a discente recebeu o conceito final: **APROVADO**. Nada mais havendo, foi lavrada a presente ata, que após lida e aprovada, foi assinada pelo(a) Presidente(a) da Comissão Examinadora.

André G. Prospero

Prof. Dr. ANDRE GONÇALVES PROSPERO

AGRADECIMENTOS

Agradeço à Deus por sempre estar comigo, guiando meus pensamentos, trazendo tranquilidade, paciência e para todas escolhas. A Nossa Senhora Aparecida que tranquilizou meu coração nos momentos de profunda angustia.

Aos meus pais, Maria Cristina Alves Pereira e Marcelo Henrique de Almeida Buranello, por todo incentivo, apoio e condições para que mais uma etapa da minha vida fosse concluída. Obrigada por serem espelho de determinação, trabalho, persistência, e principalmente amor. Deixo aqui a frases as quais ouvi com frequência em momentos de desespero: “Laís, você é filha de quem mesmo? Então vai em frente, vai trabalhar!” e “Filha, o trabalho dignifica o homem”.

As minhas irmãs Lilian Pereira Buranello e Leticia Pereira Buranello, por todo amor e felicidade transmitido mesmo a distância. Agradeço por serem minhas companheiras, a vida é mais leve com vocês. A toda minha família, especialmente aos meus avós que sempre torceram pelo meu sucesso.

Agradeço ao professor Titular José Ricardo de Arruda Miranda, por abrir as portas de seu laboratório, permitindo que eu fizesse parte do seu grupo de pesquisa. Obrigada pela orientação, pelos ensinamentos, e por deixar que eu desenvolvesse uma independência e descobrisse minha admiração pela pesquisa e pela vida acadêmica.

Agradeço ao meu coorientador Dr. André Gonçalves Próspero, o qual foi o idealizador deste projeto e tive o prazer de ter mais uma oportunidade de trabalharmos juntos. Dr. André infelizmente precisou mudar da área de atuação, mas deixou um excepcional exemplo de pesquisador, professor e pessoa. Espero ansiosamente por futuras parcerias.

Agradeço especialmente ao Me. Gabriel Gustavo de Albuquerque Biasotti, o qual foi meu parceiro oferecendo importantíssimas contribuições na execução deste projeto. Obrigada pelos ensinamentos, pela base teórica oferecida, e principalmente pela extrema paciência. Novos projetos estão por vir.

Agradeço ao Erick Guilherme Stoppa que foi meu companheiro de mestrado, o qual me ensinou sobre processos importantes para a realização deste projeto, e dividiu comigo momentos de angustia e desespero até a finalização desta fase.

Agradeço a minha amiga Ana Luiza Milani que é meu lar em Botucatu, obrigada pelo carinho, cuidado e companheirismo. Agradeço ao Mario Lucas pelos momentos de desabafos e de descontração.

Agradeço a todos meus amigos, especialmente a Samara, Isabela, Gabriela, Raissa, Marcelo e Guilherme, pela amizade construída ao longo desses anos e por todo apoio.

Agradeço aos meus companheiros do Laboratório de Biomagnetismo, especialmente ao Guilherme, Gustavo, Michael e João Miguel.

O presente trabalho foi realizado com apoio da Coordenação de Aperfeiçoamento de Pessoal de Nível Superior – Brasil (CAPES) – 30402000

Obrigada a todos que de alguma forma influenciaram na finalização de mais uma fase em minha vida.

Sumário

RESUMO

As micro e nano partículas magnéticas (MNPMs) são matérias com grande potencial para sistemas de entrega direcionada de fármaco, devido suas propriedades magnéticas e seu tamanho reduzido. Entretanto, para melhores informações e eficiência do processo de direcionamento é necessário técnicas capazes de detectar, localizar e imagiar as MNPMs dentro do organismo. Atualmente há algumas técnicas disponíveis, porém com algumas inviabilidades como alto custo, ausência de portabilidade e restrições para a experimentação animal. Desta maneira, a Biosusceptometria de Corrente Alternada (BAC) é uma técnica biomagnética capaz de detectar e realizar o imagiamento quantitativo das MNPMs *in vitro*, *ex vivo*, *in vivo* e em tempo real. Os resultados obtidos até o momento são reconstruções bidimensionais, restrita a aquisição em um único plano. Com o intuito de gerar imagens tomográficas e quantitativas utilizando a BAC, propomos um arranjo octogonal de bobinas detectoras e excitadoras disposto em uma geometria circular, possibilitando a aquisição em diferentes projeções. Esta configuração formada por múltiplas bobinas de detecção e excitação permitiu o teste de diferentes métodos e configurações de ativação das bobinas. Esses métodos permitiram uma análise mais profunda da estabilidade do problema inverso. Os resultados mostraram que a adição de bobinas de detecção resultou em uma melhor reconstrução, devido a quantidade de informações adicionadas no problema. Os resultados apresentados podem ter enormes impactos no desenvolvimento de futuras metodologias BAC que podem auxiliar no desenvolvimento de sistemas de entrega de medicamentos direcionados e possíveis aplicações *in vivo* de materiais micro e nano magnéticos.

Palavras-chave: Micro e Nano Materiais Magnéticos, Biosusceptometria de Corrente Alternada, Imagiamento Quantitativo e Tomográfico.

ABSTRACT

Micro and nano magnetic particles (MNMPs) are materials with great potential for drug delivery systems and magnetic hyperthermia agents, due to their magnetic properties and small size. However, for better targeting process efficiency, techniques capable of detecting, locating and imaging MNPMs within the organism are necessary. Currently there are some techniques available, but with some disadvantages such as high cost, lack of portability, and restrictions for animal experimentation. Thus, Alternating Current Biosusceptometry (ACB) is an alternative biomagnetic technique capable of detecting and performing quantitative imaging of MNMPs *in vitro*, *ex vivo*, *in vivo,* and in real-time. So far, the ACB results presented were restricted to quantitative planar images. To generate quantitative tomographic images using the ACB, we propose an octagonal array of pick-up and excitation coils arranged in an octagonal geometry, enabling acquisition in different projections. This configuration formed by multiple pick-up and excitation coils allowed us to test different methods and setups of coils activation. These different methods and setups enabled a deeper analysis of the ACB inverse problem stability and details. The results showed that the addition of pick-up coils resulted in a better reconstruction due to the amount of information added to the problem. Here we show for the first time the ACB quantitative tomographic reconstruction of magnetic materials distribution. The data presented here can have huge impacts on the development of future ACB methodologies that may assist in developing targeted drug delivery systems and possible *in vivo* applications of micro and nano magnetic materials.

Keywords: Micro and Nano Magnetic Materials, Alternating Current Biosusceptometry, Quantitative and Tomographic Imaging.

INTRODUÇÃO GERAL

Atualmente, as micro e nano partículas magnéticas (MNPMs) são materiais muito interessantes, principalmente em relação às suas propriedades magnéticas que possibilitam sua detecção e direcionamento dentro do organismo através da aplicação de campos magnéticos externos (1,2). Assim, as MNPMs podem ser utilizadas para investigar processos biológicos, auxiliar no diagnóstico atuando como agente de contraste de técnicas como a ressonância magnética, e no aprimoramento de técnicas terapêuticas como a hipertermia magnética (3,4,5). A capacidade de ligação entre os agentes terapêuticos e os transportadores magnéticos contribui para a administração de doses baixas e uma liberação controlada de fármacos através da redução da distribuição sistêmica (6). Desse modo, as metodologias capazes de realizar imagens quantitativas das MNPMs são necessárias para avaliar o processo e a eficiência da liberação controlada de fármacos que utilizam essas tecnologias (2).

A imagem por ressonância magnética (MRI – do inglês *Magnetic Ressonance Imaging*), o imagiamento de partículas magnéticas (MPI – do inglês *Magnetic Particle Imaging*) e o imagiamento por magnetorelaxometria (MRXI – do inglês *Magnetorelaxometry Imaging*) são técnicas empregadas na reconstrução e quantificação de distribuição de MNPMs. A MRI pode utilizar as MNPMs como agentes de contraste e, desta forma, as imagens e a quantificação são estimadas indiretamente através das alterações que esses materiais causam nas propriedades do meio (7,8). O MPI mensura a amplitude de harmônicos gerados através da resposta não linear da magnetização das MNPMs quando sob influência de campos alternados de alta amplitude e frequência (9,10). A MRXI mede o perfil de decaimento da magnetização das MNPMs após aplicar e cessar um campo magnetizante externo (11,12). Apesar das diferenças nos princípios físicos explorados, as três técnicas citadas possuem boa resolução espacial e sensibilidade. No entanto, esses métodos apresentam algumas restrições como: campo de visão (FOV – do inglês *field of view*) de tamanho limitado, alta complexidade instrumental e operacional, necessidade de ambiente magneticamente ou eletromagneticamente blindado e pouca acessibilidade para a experimentação animal, principalmente devido ao alto custo instrumental e operacional (13,14).

A Biosusceptometria de Corrente Alternada (BAC) é um método biomagnético com histórico de aplicações das MNPMs em estudos *in vitro* (15,16,17), *in vivo* (18,19,20) e

ex vivo (18,21), capaz de gerar imagens bidimensionais qualitativas (22,23) e, mais recentemente, quantitativas (24,25). O diferencial da BAC é a portabilidade, versatilidade, baixo custo instrumental e operacional, e ausência da necessidade de blindagem magnética ou eletromagnética.

Recentes avanços possibilitaram a solução do problema inverso atrelado à técnica BAC para reconstruir imagens bidimensionais e quantitativas de distribuições de nanopartículas magnéticas (NPMs) (24,25). Inicialmente foram desenvolvidas abordagens baseadas em escaneamentos planares utilizando o sensor BAC mono-canal. Essa modalidade apresentou resolução espacial milimétrica e sensibilidade de alguns miligramas de NPMs (24). Também, já foi mostrado a possibilidade da obtenção de imagens em tempo real utilizando sensores BAC de múltiplos canais. Em comparação com o método de escaneamento planar, o uso do arranjo extenso de bobinas reduz a quantidade total de sinais adquiridos. Apesar do método de múltiplos canais preservar a sensibilidade do sistema, esta modalidade reduz drasticamente a resolução espacial do sistema. A viabilidade do método BAC de múltiplos canais para ensaios *in vivo* foi apresentada em um recente estudo que mostrou a influência do carcinoma hepatocelular na biodistribuição de NPMs em modelo animal por imagens quantitativas em tempo real (26).

Apesar da boa performance nos ensaios *in vitro* e *in sílico*, além do aumento da versatilidade da técnica relacionada à capacidade de gerar imagens quantitativas, as reconstruções baseadas no problema inverso atrelado à técnica são restritas às imagens bidimensionais. Isso ocorre porque os atuais modelos instrumentais BAC apresentados até o momento foram desenvolvidos para a aquisição de sinais em uma única projeção. Dentre as propostas de aplicação da BAC existem diversos parâmetros associados à fenômenos volumétricos, como a biodistribuição *in vivo* de NPMs, ou a desintegração de comprimidos, que podem ser mal interpretados ou impossíveis de serem determinados através de imagens planares. A resolução de problemas associados à distribuição em profundidade e possíveis sobreposições de materiais podem ser alcançada através de imagens tomográficas.

A principal característica das imagens tomográficas é a reconstrução da imagem por meio de sinais adquiridos através de múltiplas projeções. As atuais limitações instrumentais da BAC para escaneamentos planares tornam a reconstrução de imagens tomográficas via BAC dependente do desenvolvimento de novos métodos para a

aquisição de sinais em diferentes arranjos e projeções. Nesse trabalho apresentamos uma nova abordagem instrumental de BAC com arranjo de sensores em formato de um octógono regular de bobinas excitadoras e detectoras (BAC8) que podem atuar independentes uma das outras. Esse modelo possibilita o controle do perfil do campo magnetizante no FOV através do sequenciamento e modulação das bobinas excitadoras e a aquisição em 8 diferentes projeções através das bobinas detectoras. A ativação dos sensores em sequenciamentos não triviais resulta no elevado número de informações não-mutuas, o que torna o problema inverso da técnica mais estável, com melhor performance e possibilita a reconstrução de imagens tomográficas. Foram propostos dois métodos de aquisição de sinais, sistema BAC8 fixo e sistema BAC8 transladando em 5 posições, e em cada método de aquisição foram aplicados 4 diferentes *setups* de ativação das bobinas. A performance dos modelos foi avaliada através de experimentações *in vitro* e *in sílico* de diferentes distribuições de ferrita de manganês micro estruturada nos FOVs utilizados. Além disso, também mostramos a possibilidade da reconstrução de imagens tomográficas com múltiplos *slices* por meio de experimentações *in sílico*.

REFERÊNCIAS

1. Dobson J. Magnetic micro-and nano-particle-based targeting for drug and gene delivery. 2006.
2. Mohseni M. Scalable strategies for tumour targeting of magnetic carriers and seeds: UCL (University College London); 2020.
3. Ortega, D., & Pankhurst, Q. A. (2013). Magnetic hyperthermia. *Nanoscience*, *1*(60), e88.
4. Sommer, W. H., Sourbron, S., Huppertz, A., Ingrisch, M., Reiser, M. F., & Zech, C. J. (2012). Contrast agents as a biological marker in magnetic resonance imaging of the liver: conventional and new approaches. *Abdominal imaging*, *37*(2), 164-179.
5. Comanescu, C. (2022). Magnetic Nanoparticles: Current Advances in Nanomedicine, Drug Delivery and MRI. *Chemistry*, *4*(3), 872-93 0.
6. Singh, A. P., Biswas, A., Shukla, A., & Maiti, P. (2019). Targeted therapy in chronic diseases using nanomaterial-based drug delivery vehicles. *Signal transduction and targeted therapy*, *4*(1), 1-21.
7. Na, H. B., Song, I. C., & Hyeon, T. (2009). Inorganic nanoparticles for MRI contrast agents. *Advanced materials*, *21*(21), 2133-2148.
8. Qiao, R., Yang, C., & Gao, M. (2009). Superparamagnetic iron oxide nanoparticles: from preparations to in vivo MRI applications. *Journal of Materials Chemistry*, *19*(35), 6274-6293.
9. Saritas, E. U., Goodwill, P. W., Croft, L. R., Konkle, J. J., Lu, K., Zheng, B., & Conolly, S. M. (2013). Magnetic particle imaging (MPI) for NMR and MRI researchers. *Journal of Magnetic Resonance*, *229*, 116-126.
10. Gleich, B., & Weizenecker, J. (2005). Tomographic imaging using the nonlinear response of magnetic particles. *Nature*, *435*(7046), 1214-1217.
11. Arsalani, S., Radon, P., Schier, P. P., Jaufenthaler, A., Liebl, M., Baumgarten, D., & Wiekhorst, F. (2022). Developing magnetorelaxometry imaging for human applications. *Physics in Medicine & Biology*.
12. Coene, A., Crevecoeur, G., & Dupre, L. (2012). Adaptive control of excitation coil arrays for targeted magnetic nanoparticle reconstruction using magnetorelaxometry. *IEEE transactions on magnetics*, *48*(11), 2842-2845.
13. Maniam, S., & Szklaruk, J. (2010). Magnetic resonance imaging: Review of imaging techniques and overview of liver imaging. *World journal of radiology*, *2*(8), 309.
14. Weizenecker, J., Gleich, B., Rahmer, J., Dahnke, H., & Borgert, J. (2009). Three-dimensional real-time in vivo magnetic particle imaging. *Physics in Medicine & Biology*, *54*(5), L1.
15. Prospero, A. G., Buranello, L. P., Fernandes, C. A., Dos Santos, L. D., Soares, G., C Rossini, B., ... & de Arruda Miranda, J. R. (2021). Corona protein impacts on alternating current biosusceptometry signal and circulation times of differently coated MnFe2O4 nanoparticles. *Nanomedicine*, *16*(24), 2189-2206.
16. Quini, C. C., Próspero, A. G., Kondiles, B. R., Chaboub, L., Hogan, M. K., Baffa, O., ... & Miranda, J. R. (2019). Development of a protocol to assess cell internalization and tissue uptake of magnetic nanoparticles by AC Biosusceptometry. *Journal of Magnetism and Magnetic Materials*, *473*, 527-533
17. Corá, L. A., Fonseca, P. R., Américo, M. F., Oliveira, R. B., Baffa, O., & Miranda, J. R. A. (2008). Influence of compression forces on tablets disintegration by AC Biosusceptometry. *European Journal of Pharmaceutics and Biopharmaceutics*, *69*(1), 372-379.
18. Quini, C. C., Próspero, A. G., Calabresi, M. F., Moretto, G. M., Zufelato, N., Krishnan, S., ... & Miranda, J. R. (2017). Real-time liver uptake and biodistribution of magnetic nanoparticles determined by AC biosusceptometry. *Nanomedicine: Nanotechnology, Biology and Medicine*, *13*(4), 1519-1529.
19. Prospero, A. G., Fidelis-de-Oliveira, P., Soares, G. A., Miranda, M. F., Pinto, L. A., Dos Santos, D. C., ... & Miranda, J. R. (2020). AC biosusceptometry and magnetic

nanoparticles to assess doxorubicin-induced kidney injury in rats. *Nanomedicine*, *15*(05), 511-525.

20. Pinto, L. A., Corá, L. A., Rodrigues, G. S., Prospero, A. G., Soares, G. A., de Andreis, U., & de Arruda Miranda, J. R. (2021). Pharmacomagnetography to evaluate the performance of magnetic enteric-coated tablets in the human gastrointestinal tract. *European Journal of Pharmaceutics and Biopharmaceutics*, *161*, 50-55.
21. Soares, G. A., Faria, J. V., Pinto, L. A., Prospero, A. G., Pereira, G. M., Stoppa, E. G., ... & Miranda, J. R. (2022). Long-Term Clearance and Biodistribution of Magnetic Nanoparticles Assessed by AC Biosusceptometry. *Materials*, *15*(6), 2121.
22. Soares, G. A., Prospero, A. G., Calabresi, M. F., Rodrigues, D. S., Simoes, L. G., Quini, C. C., ... & Miranda, J. R. (2019). Multichannel AC Biosusceptometry system to map biodistribution and assess the pharmacokinetic profile of magnetic nanoparticles by imaging. *IEEE transactions on nanobioscience*, *18*(3), 456-462
23. Corá, L. A., Andreis, U., Romeiro, F. G., Américo, M. F., Oliveira, R. B. D., Baffa, O., & Miranda, J. R. A. (2005). Magnetic images of the disintegration process of tablets in the human stomach by ac biosusceptometry. *Physics in Medicine & Biology*, *50*(23), 5523.
24. Biasotti, G. G. D. A., Próspero, A. G., Alvarez, M. D. T., Liebl, M., Pinto, L. A., Soares, G. A., ... & Miranda, J. R. D. A. (2021). 2D Quantitative Imaging of Magnetic Nanoparticles by an AC Biosusceptometry Based Scanning Approach and Inverse Problem. *Sensors*, *21*(21), 7063.
25. Soares, G., Pinto, L., Liebl, M., Biasotti, G., Prospero, A., Stoppa, E., ... & Miranda, J. R. A. (2022). Quantitative imaging of magnetic nanoparticles in an unshielded environment using a large AC susceptibility array.
26. Soares, G. A., Pereira, G. M., Romualdo, G. R., Biasotti, G. G., Stoppa, E. G., Bakuzis, A. F., ... & Miranda, J. R. (2022). Biodistribution Profile of Magnetic Nanoparticles in Cirrhosis-Associated Hepatocarcinogenesis in Rats by AC Biosusceptometry. *Pharmaceutics*, *14*(9), 1907.

ARTIGO CIENTÍFICO

1. Introduction

Micro and nanostructured magnetic materials (MNMMs) are successfully employed in a wide range of biomedical applications, mainly because of their small size and magnetic characteristics (1, 2). Also, there is the possibility to detect and control these materials within the organism by applying external magnetic fields. These materials can be applied in several tasks, including cell-separating techniques, immunoassays, drug delivery systems, and as contrast agents and magnetic tracers (2-7). In this way, biomedical applications of MNMMs require techniques to detect, locate, and quantify these materials distributed in biological tissues. Therefore, the possibility of performing images related to the delivery and localization of magnetic materials at sites of interest is very important for developing new methodologies for more effective therapies.

Some imaging systems are able to reconstruct and quantify distributions of micro and nanostructured magnetic materials. Among these, the most promising imaging systems are Magnetic Resonance Imaging (MRI) (8), Magnetic Particle Imaging (MPI) (9, 10), and Magneto Relaxometry Imaging (MRXI) techniques (11, 12). Despite their excellent performance, these systems present some disadvantages such as high complexity, lack of portability, limitations in the size of the field of view (FOV), need for the magnetic or electromagnetic shielded environment, and restrictions for animal experimentation related to high instrumental and operational costs (9, 13).

The Alternating Current Biosusceptrometry (ACB) is a biomagnetic technique that detects micro and nanostructured magnetic materials *in vivo*, *in vitro*, and *ex vivo* (14-18). The ACB is a portable and versatile system, already available for *in vivo* and real-time detection of magnetic materials, which allows better investigations of the magnetic materials behavior of the within the organism. In the past, the ACB system was able to perform qualitative imaging of magnetic materials *in vivo* and real-time (19, 20). Recently, our group presented an inverse problem solution related to the ACB system (single channel and multi-sensor), allowing quantitative 2D reconstructions of magnetic material distributions in gypsum phantoms (21, 22). To date, there are two main imaging methodologies related to the ACB system: i) the spatial plot of ACB signal intensity, which is a simple methodology and results in qualitative images, and ii) solving the inverse problem related to the ACB system, which is a more complex methodology, but resulting in quantitative images. It is important to mention that both methodologies presented so far are restricted to reconstructing only 2D distributions of magnetic materials. Thus, there is still a lack of methodologies

able to perform quantitative tomographic imaging of micro and nanostructured magnetic materials using the ACB system.

The inverse problem solution related to the ACB system allows estimating the position and the mass of magnetic materials distributed in a determined FOV from a set of acquired signals (21). This result is achieved by solving a set of equations that describe the ACB system response to materials distributions in the voxels of the FOV. The problem stability and its reconstruction accuracy hardly depend on ACB signal acquisition methodology. To reconstruct quantitative tomographic images of the distribution of MNMMs using the ACB system, it is necessary to modify its current signal acquisition methodology.

Several methods were reported to improve the reconstruction efficiency of similar imaging systems, such as the use of multiple excitation fields (which increases information regarding the positioning and quantity of magnetic materials) (11), the parameters optimization related to the inverse problem stability that results in the best choice of excitation coil activation sequence (23), and selecting optimal configurations of magnetic fields, excitation coil and sensor positioning (24).

The current ACB acquisition methodology is based on a FOV scanning where the sensors' axis is perpendicular to the FOV's plane. Here, we propose a different ACB setup based on a different acquisition approach to reconstruct tomographic images of magnetic materials distributions. In such an approach, the sensor is arranged in an regular octagonal array of coils, where their axes are parallel to the FOV plane to obtain different projections of the magnetic material distribution. Also, the new setup is composed of multiple pick-up and excitation coils, which allowed us to record information in several different projections and employ different methods to improve the inverse problem stability and, consequently, the reconstruction quality.

2. Materials and Method

2.1 ACB Octagonal System

The ACB single channel (ACB-SC) sensor is composed of two pairs of exciting and pick-up coils, as shown in Figure 1A-1B, which works as a double magnetic flux transformer. When there is a magnetic material near the pick-up coils, an unbalance of the system's magnetic flux occurs, and a corresponding electrical signal is generated. This signal can be recorded using a *lock-in* amplifier, an analog-to-digital (A/D) board and a computer. The electric signal intensity depends on the distance between the sensor and the magnetic sample, coil's geometries, electronic parameters, and the amount and magnetic susceptibility of the magnetic material.

In this work, we developed an ACB Octagonal System (ACB8), composed of an array of eight ACB-SC sensors positioned in a regular octagonal geometry around a circle with a radius of 4 *cm* (Figure 1C). The excitation coils system is independent, so the coils can be activated in many different sequences. Also, the system is built in a way that the pick-up coils can acquire the signal from magnetized materials inside the central circle regardless of which excitation coils setup is active. The excitation coils were built with 280 turns of AWG 24 copper wire, with an inner diameter of 2,5 *cm*. The pick-up coils were built with 560 turns of AWG 36 copper wire, with an inner diameter of 2 *cm*. The baseline between the excitation and pick-up coils pairs is 15 *cm*.

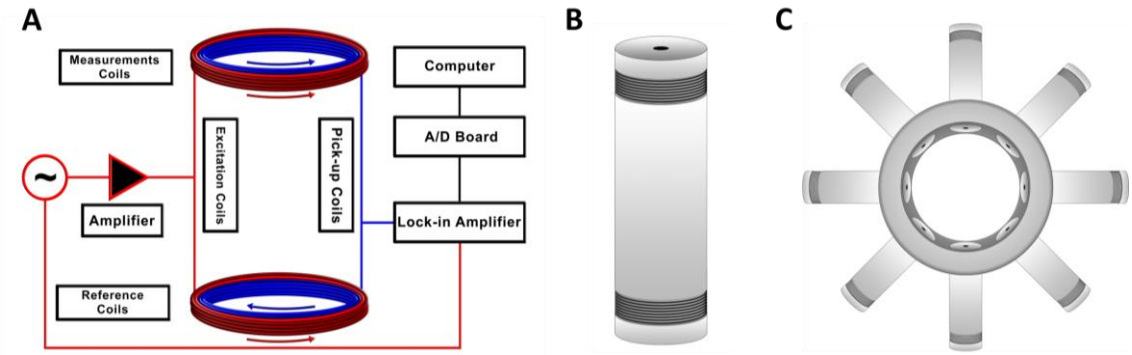

Figure 1. (A) Schematic representation of the Alternate Current Biosusceptometry (ACB) system. The blue rows indicate the pick-up coils, and red rows indicate the excitation coils. (B) Representation of the ACB single channel sensor (ACB-SC). (C) Representation ACB Octagonal System composed of an array of eight ACB-SC sensors positioned in a regular octagonal geometry.

2.2 Forward Problem and Solution of Inverse Problem

The inverse problem related to the reconstruction of magnetic materials sensordBo atdistributions is commonly classified as an ill-conditioned problem. This is related to the fact that the problem can have many solutions (many magnetic material distributions which can generate the same set of intensity

signals), or the solution procedure is unstable, where small errors in the data, related to the measurement procedure, can be amplified resulting in large errors in the solution. In this way, the solution's stability can be strongly dependent on the ratio between the number of information (equations) and the number of unknowns, and the quality of this information (i.e., repeated, similar or inaccurate information can deteriorate the solution).

Here, we tested four different methodologies for the ACB8 signal acquisition, as described in the section 2.4. Each of the methodologies comprises a different set of information (with different quality and number of information) used to reconstruct the magnetic materials distribution. Therefore, to mathematically describe the new ACB8 system and its acquisition methodologies, let N_k be the number of voxels to be imaged, N_p and N_e the number of pick-up and excitation coils employed in the *a*-th methodology, respectively. Consequently, the ACB forward model described by Biasotti et. al (2021), can be formulated as

$$\boldsymbol{V_a} = \boldsymbol{L_a}.\boldsymbol{X_{TM}} \qquad (1)$$

where $\boldsymbol{V_a} \in \mathbb{R}^{N_eN_p}$ is the induced signal vector, $\boldsymbol{L_a} \in \mathbb{R}^{N_eN_p \times N_k}$ is the sensitivity matrix of the system and $\boldsymbol{X_{TM}} \in \mathbb{R}^{N_k}$ is the amount of magnetic material vector that represents the distribution of magnetic material in the *k* voxels of the imaged FOV (21, 24). The sensitivity matrix elements of the ACB8 system related to the acquisition methodology *a*, are given by

$$L_{n,s,k} = \frac{1}{\sqrt{2}} \frac{|\chi_m|\omega}{\mu_0 I_r} \left(\boldsymbol{B_{m_{n,k}}} \cdot \boldsymbol{B_{r_{s,k}}} \right) \qquad (2)$$

where χ_m is the mass magnetic susceptibility, ω is the angular frequency of the alternating current, μ_0 is the magnetic permeability in the vacuum, I_r is the reciprocal current, $\boldsymbol{B_{m_{n,k}}}$ is the magnetizing field amplitude of the *n*-th excitation coil, and $\boldsymbol{B_{r_{s,k}}}$ is the reciprocal field of the *s*-th pick-up coil, in the *k*-th voxel, when using the acquisition methodology *a*.

There are several linear optimization techniques to estimate the most probable solution of an inverse problem. Here, we employed the determination of the Moore-Penrose pseudo-inverse matrix ($\boldsymbol{L^+} = (\boldsymbol{L^T L})^{-1}\boldsymbol{L^T}$), applying the Truncated Singular Value Decomposition (TSVD) regularization method to estimate the inverse matrix $\boldsymbol{L^+}$, as described previously (21, 25). Thus, the ACB inverse problem solution is given by

$$\boldsymbol{X_{TM}} = \boldsymbol{L^+ V} \qquad (3)$$

2.3 Calculated Sensitivity Matrix and its Calibration

The calculated sensitivity matrix $\boldsymbol{L_{cal}}$ was built in *in silico*, as previously described by our group. Briefly, we employed the Hanson and Hirshman`s computationally efficient expressions for the Biot-Savart field of filamentary segments to calculate both $\boldsymbol{B_{m_{n,k}}}$ and $\boldsymbol{B_{r_{s,k}}}$, and consequently to calculate each $L_{n,s,k}$ element of each $\boldsymbol{L_{cal}}$ matrix (26). Each turn of each coil was approximated by 36 rectilinear segments, which results in calculation errors below 1% (25). Also, the magnetic field at a specific location was the sum of magnetic fields from all rectilinear segments.

The $\boldsymbol{L_{cal}}$ matrix elements are composed by the magnetic field amplitudes and constant values of frequency, current, magnetic permeability in the vacuum, mass magnetic susceptibility, and, when using an A/D board, there is a conversion factor that must be considered. Also, it is interesting to include the system`s noise to the problem. Despite these factors be calculable, here we experimentally determined a calibration factor representing all these constant values together. Thus, we experimentally recorded (using the A/D board) the response of all detectors when a phantom of $MnFe_2O_4$ ($400\ mg$) was placed in in the central voxel of the FOV. This process was performed repeatedly until reaching a convergence of values, and the mean value obtained was chosen as the calibration factor. The calibration factor represented the variability of each sensor response and was employed as a multiplicative correction factor.

The calculations were performed by each voxel position, and each voxel was subdivided into 125 calculation points to account for the magnetic gradient field within each voxel. Note that the 125 points are distributes in both horizontal and vertical directions of the voxel, and the mean values of these 125 points represented one voxel, which in its turn composes one tomographic slice.

It is important to mention that our group previously showed that the $\boldsymbol{L_{cal}}$ mathematical-computational method presented good and valuable results, and could be employed to replace the experimental determination of the $\boldsymbol{L}$ matrix (21). Also, this method is much less time and material consuming, and is less susceptible to experimental inaccuracies.

2.4 Coils Setups and Positioning for Signal Acquisition

We tested four different coil setups and two different system positioning methods for the ACB8 system, resulting in eight different signal acquisition methods. The setups were based on the amount of excitation and pick-up coils simultaneously active, and the positioning methods are based on a single static acquisition (fixed method, shown in Figure 2A) or an acquisition in which the system is translated 1 cm in five different positions (center, right, left, forward

and backward – translated method, shown in Figure 2B), with one complete acquisition in each position.The single static acquisition method enabled a FOV with a volume of 7 x 7 x 1 cm^3 , subdivided into 37 isovolumetric voxels of 1 cm^3, while the acquisition with the system translated enabled a 5 x 5 x 1 cm^3 FOV, subdivided in 21 voxels isovolumetric voxels of 1 cm^3. In both cases, each voxel was subdivided into 125 calculation points to account for the magnetic gradient field inside one voxel.

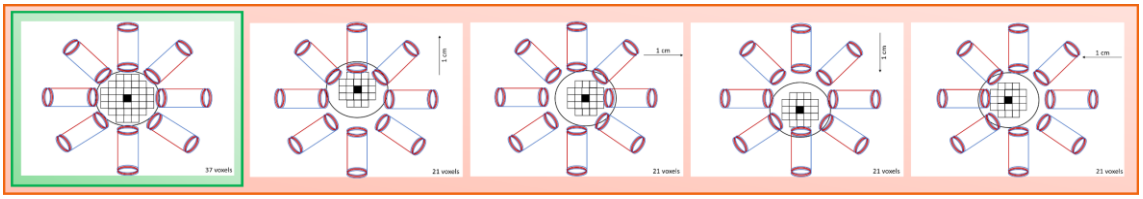

Figure 2. Schematic representation of the two different system positioning methods for the ACB8 system.The green square shows the system configuration for performing the fixed method, with FOV subdivided in 37 voxels.The orange squares shows system configuration for performing the translated method, wich is shifted 1 cm to five different positions (center, forward, righ, backward and left), with FOV subdivided in 21 voxels.

The coils setups studied are described below:

Coil setup 1 (*CS1*): the eight sensors were activated in sequence, where only one sensor was active at a time, as shown in Figure 3 (first row in blue). 5 s of signal acquisition were performed by each sensor, and the mean value obtained for each sensor was used in the reconstruction algorithm. This setup made available a sensitive matrix with dimensions of $\boldsymbol{L} \in \mathbb{R}^{8\times37}$.

Coil setup 2 (*CS2*): this setup was the same as the Coil setup 1, but with the opposite excitation coil also active (Figure 3, second row in orange). This method was implemented to increase the magnetic field amplitude in the FOV's center. Thus, the setup 2 also resulted in a sensitive matrix with dimensions of $L \in \mathbb{R}^{8\times37}$.

Coil setup 3 (*CS3*): eight excitation coil pairs were activated in sequence, with six pick-up coils simultaneously active when each excitation coil was active. In this method, the signals of the two neighboring pick-up coils of the active excitation coil were discarded in the reconstruction due to a very low-quality information they added in the inverse problem (Figure 3, third row in green). This method resulted in a sensitive matrix with dimensions of $L \in \mathbb{R}^{48\times37}$.

Coil setup 4 (*CS4*): this setup was the same as the *CS3*, but with the opposite excitation coil also active. As the opposite excitation coil was also active, we discarded the signals from four pick-up coils: two neighboring pick-up coils of each of the two excitation coils active (Figure 3, fourth row in yellow). This method resulted in a sensitive matrix with dimensions of $L \in \mathbb{R}^{16\times37}$. Note that

the projections 5, 6, 7 and 8 were discarded because of the symmetry to the projections 1, 2, 3 and 4.

When using the translated method, one can multiply the number of sensors by five in each coil setup presented. Thus, we obtained sensitivity matrices with dimensions of $L \in \mathbb{R}^{40\times21}$, $L \in \mathbb{R}^{40\times21}$, $L \in \mathbb{R}^{240\times21}$, and $L \in \mathbb{R}^{80\times21}$.

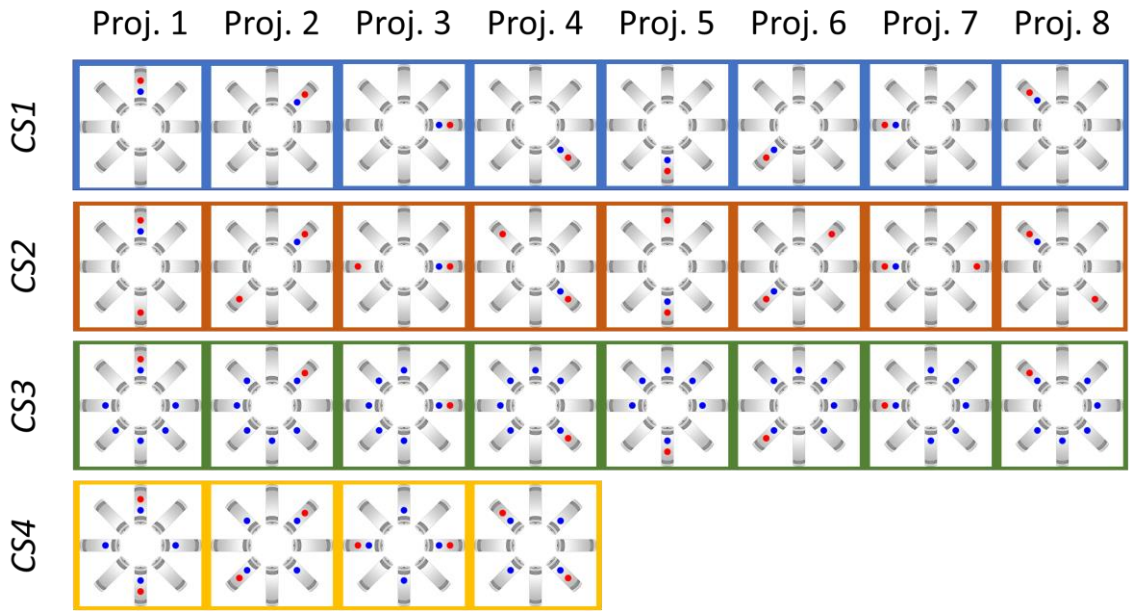

Figure 3. Schematic representation of the coil's setups for signal acquisition. Each row shows a specific coil setup (*CS*): *CS1* - blue; *CS2* - orange; *CS3* - green; and *CS4* - yellow. In the columns are represented the coils activation sequence and projection for each setup: blue circles represent active pick-up coils, while red circles represent active excitation coils.

2.5 Evaluation of Inverse Problem Stability

We evaluated the inverse problem stability through two figures of merit: the homogeneity of system's spatial sensitivity and the condition number of the sensitivity matrix.

The sensitivity map measures the absolute response of the system to a material positioned in each of the voxels and is given by

$$\boldsymbol{S} = \left[\sum_{i=0}^{N_p N_a} |L_{i,0}|, \sum_{i=0}^{N_p N_a} |L_{i,1}|, \dots, \sum_{i=0}^{N_p N_a} |L_{i,k}| \right] \quad (4)$$

The homogeneity of spatial sensitivity is represented as the variation coefficient of the sensitivity map, and is calculated as

$$CV(\boldsymbol{S}) = \frac{STD(\boldsymbol{S})}{\mu(\boldsymbol{S})} \quad (5)$$

where $STD(\boldsymbol{S})$ is the standard deviation and $\mu(\boldsymbol{S})$ is the mean value of $\boldsymbol{S}$. The inhomogeneity across the FOV reduces the inverse problem stability due to the

amplifications of errors associated with inhomogeneous distributions of mass inside the voxels, and imprecisions in the positions of the phantoms.

The condition number is a commonly employed method to evaluate the inverse problem stability, and was widely employed in similar studies (27, 28). This parameter can be calculated as

$$\kappa(\boldsymbol{L}) = \frac{\max(\boldsymbol{\sigma}(\boldsymbol{L}))}{\min(\boldsymbol{\sigma}(\boldsymbol{L}))} \qquad (6)$$

where $\boldsymbol{\sigma}$ is the vector of $\boldsymbol{L}$ matrix singular values. High values of $\kappa(\boldsymbol{L})$ are associated to more instable solutions, i.e., the solution is more susceptible to perturbations in the measured signal (intrinsic system noise, and imprecisions in instrumental and operational processes).

2.6 Evaluation of ACB-8 Performance and Validation of in silico Model

2.6.1 Models of Magnetic Material Distribution

We built test phantoms made of manganese ferrite ($MnFe_2O_4$) microparticles ($50 - 100\ \mu m$). The phantoms were immobilized in gypsum, using different magnetic material amounts. We built five cube phantoms with dimensions of $1 \times 1 \times 1\ cm^3$containing 400 mg of manganese ferrite microparticles, and a bar phantom with dimensions of $3 \times 1 \times 1\ cm^3$ containing $3000\ mg$ of manganese ferrite microparticles. We employed the cube phantoms in two different combinations to form different distributions of magnetic material in the FOV. The phantoms were combined and placed in different configurations in the FOV, as described in the next section.

2.6.2 In vitro Assays

To evaluate the performance of the proposed methods in the reconstruction, we combined the cube phantoms in different geometries along the FOV. As the coils setups and the system positioning methods (fixed and translated methods) enabled different FOV dimensions, we employed different phantom combinations in each case.

For the fixed method, we used 8 different phantom distributions: two cubes placed with the face-to-face distance of 1, 3, and 5 cm (combinations A, B, and C, respectively); two phantom bars placed vertically in the FOV with distances of 1 and 3 cm between the bars' surfaces (D and E, respectively); two phantom bars placed horizontally with distances of 1 and 3 cm between the bars' surfaces (F and G, respectively); and a cross formed by five cube phantoms positioned in the center of the FOV (H). For the translated method, we studied 3 different phantom

distributions: one bar positioned vertically at the center of the FOV; one bar positioned horizontally at the center of the FOV, and a cross using five cubes in the center of the FOV (A, B, and C, respectively).

2.6.3 In silico Assays

The same distributions studied in the *in vitro* assays were simulated to calculate the *in silico* signals. Through simulations, the induced voltage was calculated in each of the detectors by solving the forward problem (using the Hanson and Hirshman method, and also the calibration factor we determined, as described before), considering the specific parameters of each acquisition method, and the coordinates and distributions of magnetic material in the voxels. To obtain a more realistic situation, we added the ACB8 realistic noise in the calculations, as described by Coene et al., 2014 (29). The results calculated *in silico* were compared with the results obtained *in vitro* to verify the efficacy and realness of the *in silico* experiments for future works.

2.7 Parameters for imaging quality evaluation

The imaging quality was assessed by the quantification precision and the geometric quality of the reconstructed images (27, 30). The quantification precision was calculated as the absolute relative difference (X_{diff}) percentage between the sum of the estimated magnetic material mass ($X_{est,tot}$) in the k voxels in the reconstructed images, and the sum of nominal mass in the k voxels of the FOVs ($X_{nom,tot}$). Thus, X_{diff} can be calculated as

$$X_{diff} = \left| \frac{X_{est,tot}}{X_{nom,tot}} - 1 \right| . 100\% \qquad (7)$$

Person's correlation coefficient (*CC*) was calculated to verify the linear correlation between the estimated ($\bar{\boldsymbol{X}}_{\boldsymbol{est}}$) and nominal ($\bar{\boldsymbol{X}}_{\boldsymbol{nom}}$) distribution vectors, which contains the amount of magnetic material in each voxel of the reconstructed and nominal distributions, respectively. The Pearson coefficient represent the geometric quality of the reconstructions, and was determined by

$$CC = \left| \frac{\sum_k (X_{est,k} - \bar{\boldsymbol{X}}_{\boldsymbol{est}}).(X_{nom,k} - \bar{\boldsymbol{X}}_{\boldsymbol{nom}})}{\sqrt{\sum_k (X_{est,k} - \bar{\boldsymbol{X}}_{\boldsymbol{est}})^2}.\sqrt{\sum_k (X_{nom,k} - \bar{\boldsymbol{X}}_{\boldsymbol{nom}})^2}} \right| \qquad (8)$$

3. Results

3.1.Stability of Inverse Problem Solution

The Figure 4 shows the sensitivity map for each acquisition method (fixed and translated) and coils setups (1, 2, 3, and 4). In all of the maps it is possible to

observe that there is a profile of a low sensitivity in the FOV's central areas and high sensitivity in its the peripheries. As the fixed method has a larger FOV and a larger distance between the sensors and the central voxels, it presents a higher gradient in radial sensitivity. In the other hand, the translated method has a smaller FOV (because of the translational approach, which shrank the FOV dimensions in 1 cm in each of the translated directions), and consequently, the gradient in radial sensitivity is lower. Note that the difference between the sensitivity maps scales is associated to the differences in the number of signals acquired by each method (number of pick-up coils with high quality information, i.e., not discarded), and the increase of magnetizing field intensity when more than 1 exciting coil is active.

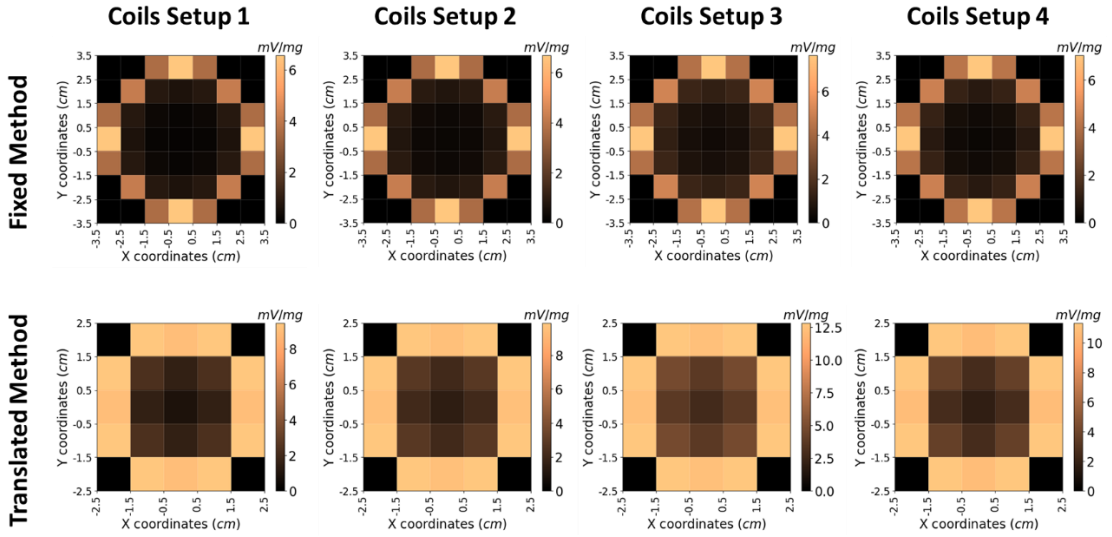

Figure 4. Sensitivity maps of the two different system positioning methods (fixed and translated method) are shown in each row, for each coils setup in each column. The first row shows the fixed method a FOV of $7 \times 7 \times 7\ cm^3$, and second row shows the translated method a FOV of $5 \times 5 \times 5\ cm^3$.

The homogeneity of spatial sensitivity along the FOV is represented as the variation coefficient of the sensitivity map, shown in Table 1. In accordance to the sensitivity map image, the fixed method has a lower homogeneity of spatial sensitivity (higher gradient in radial sensitivity) when compared to translated method, for all of the coil's setups. In both acquisition methods, the *CS2* shown a smaller CV value, i.e., an increase of homogeneity, when compared to $CS1$. This behavior was expected due to the use of the opposite excitation coil, which increases the magnetizing field homogeneity in the FOV. On the other hand, the homogeneity of spatial sensitivity is higher for the *CS3* than for the *CS2*. In this case, the homogeneity improvement is related to the use of multiples pick-up coils at the same time, which increases the reciprocal field (detecting field) homogeneity in the FOV. The CV value found for *CS4*, is higher than for *CS3*, indicating a loss of homogeneity in its FOV. This happens because of the

reduction from 6 to 4 pick-up coils, which was not compensated by the increase of magnetizing field homogeneity (two excitation coils in this case). Since the inverse problem stability is strongly dependent of the FOV's spatial sensitivity homogeneity, the *CS3* is the best option according to the CV values.

In addition to coefficient of variation, Table 1 also shows the number of condition ($\boldsymbol{k}$) found for each method and setup, which is related to the inverse problem stability. We obtained the same values of $\boldsymbol{k}$ for both *CS1* and *CS2*. For the *CS3*, we found a huge increase in the $\boldsymbol{k}$ value. When using the *CS4*, the $\boldsymbol{k}$ value was higher than for *CS1* and *CS2*, but lower than for *CS3*. This result indicates that the $\boldsymbol{k}$ parameter is strongly dependent of the number of acquired signals and the differences in signal intensity for different sensors (as higher is the difference between the maximum and minimum signal intensities detected by the most sensitive and less sensitive sensors, respectively, in the same method, the higher is the $\boldsymbol{k}$ value for this method). More specifically in the case of the *CS3*, the pick-up coils far from active excitation coils show a very low signal intensity when compared to the closer pick-up coils. Thus, analyzing the $\boldsymbol{k}$ values, the *CS3* presents the lowest stability in inverse problem solution. This happens mainly because of the high impact of the system intrinsic perturbations and the experimental inaccuracies in the low-signal channels. However, we emphasize that even the *CS1* and *CS2* showed the highest stabilities in inverse problem, these sequences carry a low number of information, and the solution may not converge to a good solution.

Table 1. CV and κ values of each positioning method for each coils setup (CS). Coefficient of variation (CV) shows the spatial homogeneity of the system, and κ shows the number of conditions of the sensitivity matrix.

Method	$\boldsymbol{CV}$				$\boldsymbol{\kappa}$			
	$\boldsymbol{CS\ 1}$	$\boldsymbol{CS\ 2}$	$\boldsymbol{CS\ 3}$	$\boldsymbol{CS\ 4}$	$\boldsymbol{CS\ 1}$	$\boldsymbol{CS\ 2}$	$\boldsymbol{CS\ 3}$	$\boldsymbol{CS\ 4}$
Fixed	0.95	0.91	0.80	0.85	1.88	1.88	19076.65	602.95
Translated	0.61	0.56	0.47	0.53	7745.43	1718.10	580.58	796.99

3.2. *Fixed Method*

Figure 5 shows the reconstruction results for the fixed method, while Tables 2 and 3 show the X_{diff} and *CC* values obtained for the *in vitro* experiments and *in silico* calculations, respectively.

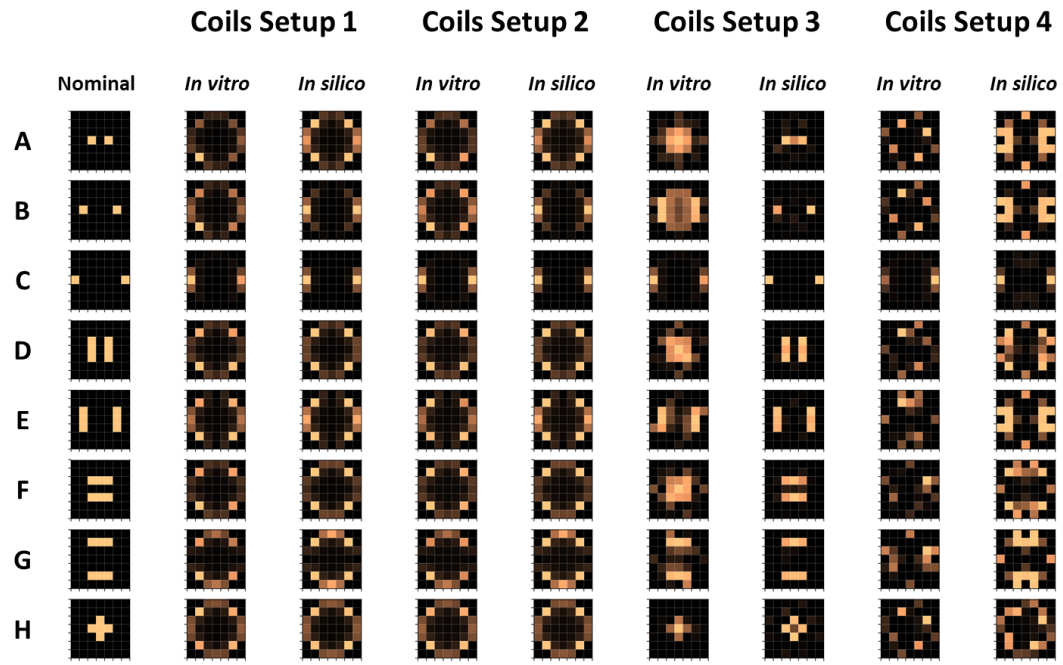

Figure 5. *In vitro* and *in silico* reconstructed images of different distribution of manganese ferrite microparticles in the FOV using the fixed method for each coil setup. The row shows the different distributions used, where the mass was varied (A, B, C - 800 mg; D, E and F – 6000 mg; G and H – 2000 mg).

Table 2. CC and X_{diff} values for the *in vitro* reconstructions of the signal of different distributions of manganese ferrite microparticles in the FOV

Distribution	X_{nom} (mg)	X_{diff} (%)				CC			
		$CS\ 1$	$CS\ 2$	$CS\ 3$	$CS\ 4$	$CS\ 1$	$CS\ 2$	$CS\ 3$	$CS\ 4$
A	800	97.19	95.56	70.40	94.63	-0.18	-0.19	0.40	0.00
B	800	94.49	89.16	36.79	88.80	-0.15	-0.15	0.39	-0.07
C	800	88.01	79.01	87.82	83.02	0.85	0.86	0.85	0.81
D	6000	91.87	85.28	18.68	87.66	-0.31	-0.30	0.61	-0.04
E	6000	76.50	65.12	27.93	72.10	-0.17	-0.17	0.84	-0.54
F	6000	91.92	84.67	18.10	87.88	-0.31	-0.31	0.60	-0.05
G	6000	75.42	65.12	27.72	72.50	-0.17	-0.17	0.83	-0.55
H	2000	95.25	89.88	2.74	91.54	-0.36	-0.35	0.94	-0.01

Table 3. CC and X_{diff} values for the *in silico* reconstructions of the signal of different distributions of manganese ferrite microparticles in the FOV

Distribution	X_{nom} (mg)	X_{diff} (%)				CC			
		$CS\,1$	$CS\,2$	$CS\,3$	$CS\,4$	$CS\,1$	$CS\,2$	$CS\,3$	$CS\,4$
A	800	95.01	92.17	2.96	92.02	-0.20	-0.20	0.83	0.05
B	800	85.46	83.40	0.92	83.24	-0.07	-0.07	0.96	0.30
C	800	30.76	32.36	5.27	32.46	0.86	0.86	1.00	0.90
D	6000	92.96	90.22	0.24	90.20	-0.32	-0.32	0.99	-0.16
E	6000	79.81	77.64	0.20	77.62	-0.18	-0.17	0.99	0.54
F	6000	92.95	90.22	0.39	90.20	-0.32	-0.32	0.98	-0.17
G	6000	79.80	77.63	0.81	77.61	-0.18	-0.17	0.99	0.54
H	2000	95.22	92.36	9.27	92.26	-0.36	-0.35	0.92	-0.15

As shown in Figure 4 the fixed method presented the highest heterogeneities in the sensitivity maps for all coils setups. Therefore, it is possible to note that Figure 5 shows a low geometrical accuracy in reconstructing the most magnetic materials geometry for all of the coil's setups, except for the *CS3 in silico* ($X_{diff} < 10\%$ and $CC > 0.8$ – Table 3). Analyzing Figure 5, Table 2 and 3, we noticed that the *CS1*, *CS2* and *CS4* presented the lowest performance to quantify and reconstruct tomographic distributions, even in low perturbation conditions such as in the *in silico* environment. In such cases, probably the ratio between the number of acquired signals (information added to the problem) and voxels to be determined (unknowns) did not allow a better convergence of reconstruction to the nominal distribution. As commented before, the *CS3* showed the highest reconstruction performance (in terms of image quality, X_{diff} and *CC* values) for all magnetic materials distributions, probably due to the highest number of simultaneous activated pick-up coils employed and amount of information added to the problem. Note that for the *CS3* the sensitivity matrix presents dimensions of $L \in \mathbb{R}^{48\times37}$, while the dimensions are $L \in \mathbb{R}^{8\times37}$, $L \in \mathbb{R}^{8\times37}$, $L \in \mathbb{R}^{16\times37}$, for the *CS1*, *CS2*, and *CS4*, respectively.

The *CS3 in vitro* was able to reconstruct some distributions with relative accuracy (C and H distributions), but the method performance is lower for the other distributions. However, the *CS3 in silico* results showed a very good performance in reconstructing all of the distributions. The differences between the *in vitro* and *in silico* results for the *CS3* is related to the stability characteristics of the inverse problem solution presented in the previous section ($\boldsymbol{k}$ values). It is important to note that in our study, the *in silico* calculations considered the system's realistic noise conditions. Thus, in accordance with the $\boldsymbol{k}$ values presented in the previous section ($\boldsymbol{k}$ = 19076.65), the *CS3* results presented in Figure 5 confirms that this

setup is more susceptible to inaccuracies of the experimental conditions. It is important to mention that even the *CS4* presenting a higher magnetizing field in the FOVs center (two excitation coils active simultaneously – the sensor's one and the opposite one), the fact of discarding the signals from the neighboring pick-up coils decreases the amount of information to the problem. Thus, this result lead to the conclusion that the amount of information added to the problem is more important than the magnetic field intensity for the sensitivity map homogeneity and consequent reconstruction quality.

3.3. Translated Method

Figure 6 shows the nominal and reconstructed distributions of magnetic materials for all of the coil's setup and phantoms studied in the translated method case. Tables 4 and 5 show the X_{diff} and *CC* values obtained for the *in vitro* experiments and *in silico* calculations, respectively, for the translated method as well.

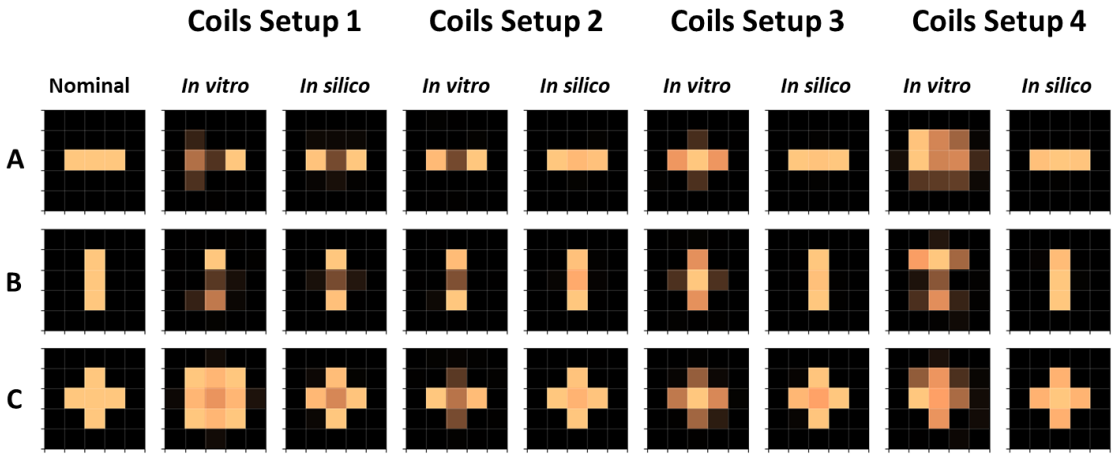

Figure 6. *In vitro* and *in silico* reconstructed images of different distributions of manganese ferrite microparticles in the FOV using the translated method for each coil setup. The row shows the different distributions used, where the mass was varied (A and B - 3000 mg, C – 2000 mg).

Table 4. CC and X_{diff} values for the *in vitro* reconstructions using translated method of the signal of different distributions of manganese ferrite microparticles in the FOV.

Distribution	X_{nom} (mg)	X_{diff} (%)				CC			
		CS 1	CS 2	CS 3	CS 4	CS 1	CS 2	CS 3	CS 4
A	3000	1.15	54.50	24.73	4.95	0.84	0.92	0.95	0.62
B	3000	5.11	56.87	25.23	4.51	0.87	0.94	0.94	0.70
C	2000	10.36	38.71	3.22	12.18	0.58	0.88	0.94	0.91

Table 5. CC and X_{diff} values for the *in silico* reconstructions using translated method of the signal of different distributions of manganese ferrite microparticles in the FOV.

Distribution	X_{nom} (mg)	X_{diff} (%)				CC			
		$CS\ 1$	$CS\ 2$	$CS\ 3$	$CS\ 4$	$CS\ 1$	$CS\ 2$	$CS\ 3$	$CS\ 4$
A	3000	6.88	0.86	0.87	0.05	0.92	1.00	1.00	1.00
B	3000	5.73	1.02	0.89	0.15	0.92	1.00	1.00	1.00
C	2000	2.79	1.00	1.15	0.40	0.99	1.00	1.00	1.00

The results obtained for the translated method are far more exciting than for the fixed method. In the case of the translated method, there are more information with relevant quality added to the problem, thus increasing the reconstruction quality and accuracy. It is important to mention that despite the higher number of information added to the problem (times five when compared to the fixed method), when using the translational method, both excitation and detection coils approximate to the central voxels of the FOV, increasing the system's sensitivity in this region, which improves the quality of the information added to the problem. For the translated method, in terms of image quality, the *CS3* presented the best results again, in both *in vitro* and *in silico* situations, with and $CC > 0.93$ for the *in vitro* experiments, and $CC = 1$ for the *in silico* calculations. As commented before, the better results achieved with *CS3* method is related to the higher information added the problem ($L \in \mathbb{R}^{240\times21}$), and also the differences between the *in vitro* experiments and *in silico* calculations are related to the inverse problem stability ($\boldsymbol{k}$ = 580.58) and consequent impacts of experimental inaccuracies in the solution obtaining process. When comparing the $\boldsymbol{k}$ values obtained for the fixed and translated methods, it is possible to observe that for fixed method the *CS3* $\boldsymbol{k}$ value was the larger one, while for the translated method it was the lowest one, probably due to the number of high-quality information added to the problem. Furthermore, all of the setups presented relative better CC and X_{diff} results for the translated method than for the fixed method.

Figure 7 shows a comparison between the fixed and translated methods in the case of the distribution phantom composed by five cubes forming a cross shape. It is possible to see that the translated method presented a superior reconstruction quality in almost all of the setups and for both *in vitro* experiments and *in silico* calculations. These results are also corroborated by the X_{diff} and CC values presented in the Tables 2, 3, 4, and 5. As expected, the translated method added information to the problem and also improved the sensitivity map homogeneity, which had huge impacts on the reconstruction quality.

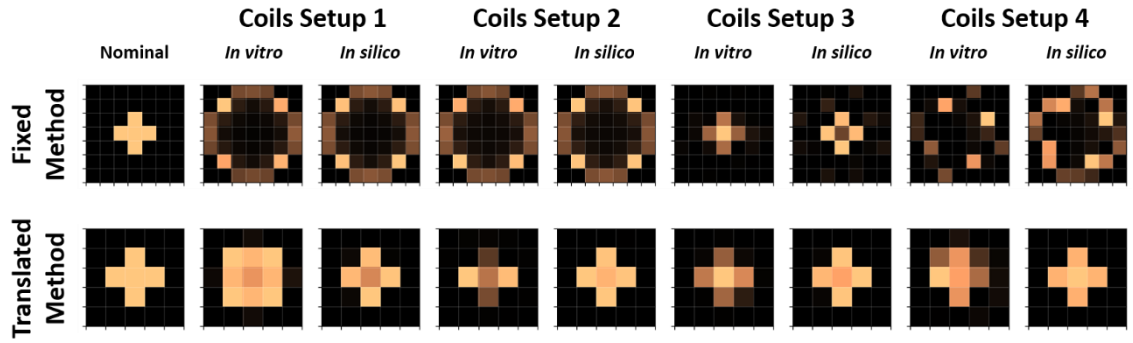

Figure 7. In vitro and in silico reconstructed images of distributions of manganese ferrite microparticles in the cross geometry using the fixed and translated method for each coil setup. The phantom cross has 2000 mg of manganese ferrite microparticles.

4. Discussion and Conclusion

Techniques capable of reconstruct spatial distributions of micro and nanomagnetic materials non-destructively brings attention of the scientific community, mainly because of its potential of determining the fate of these materials within the body (31). The possibility of performing quantitative imaging of MMNMs *in vivo* is of paramount importance for the efficiency assessment in several biomedical applications of these materials, such as drug delivery systems and magnetic hyperthermia (32, 33). To date, there are few techniques with high potential for *in vivo* quantitative imaging of MNMMs, where the most promising are the MPI , MRXI , MRI and Magnetic Susceptibility Imaging (10, 34-37). Despite these techniques present good sensitivity and spatial resolution, they also involve high costs and complexity, which limits them to be widely studied and applied (specially in animal experiments) (21).

In the past few years, our group published some papers showing the ACB system as a new alternative technique for magnetic materials *in vivo* and real-time imaging (20, 38). In such studies, the ACB presented good and valuable data. Comparing to other biomagnetic techniques, is simpler, more versatile, does not need shielded environment, and presents low operational and instrumental costs. More recently, we proposed two ACB setups and their respective inverse problem solutions, which resulted in quantitative planar reconstructions of magnetic nanoparticles (21, 22). The first setup was based on a scanning approach, where the system was able to perform planar images with at least 1 cm^{-1} of spatial resolution. Despite the system presented a very good spatial resolution, the system presented a relative large acquisition time and the possibility of only performing planar images. The second setup was based on a static system composed by two excitation coils and several pick-up coils simultaneously active, which hugely decreased the acquisition time of the ACB

system. Still, there is a lack of performing tomographic imaging of magnetic materials using the ACB system.

In this work, we developed a new setup of the ACB system (ACB8) to perform quantitative tomographic imaging of magnetic microparticles. The new setup is based on eight independent sensors arranged in a regular octagonal geometry, which enables different combinations of pick-up and excitation coils activation. Since the ACB8 allows to activate different coils simultaneously, we studied the performance of four different sequence setups of coils activation, and two types of signal acquisition method: sensor fixed and translating through five positions. Furthermore, we evaluated the inverse problem stability through the analysis of spatial sensitivity homogeneity and the condition number, i.e., the impact of experimental perturbations in the inverse solution. We found that the central area of the FOV presents the lowest sensitivity for all of the four coils setups, which was expected because of the ACB signal intensity decay profile with the distance. Previously our group showed a signal decay factor of r^{-6} for distances greater than 2 cm between the sensor surface and the detected material (39, 40). This sensitivity differences between the central voxels and the peripheral ones (sensitivity maps inhomogeneities) induces a high instability in the inverse problem solution process, which is strongly related to the high signal variations caused by the imprecisions in the magnetic material radial position. This characteristic reflects in the lower performance found for the *in vitro* experiments when compared to the *in silico* calculations, which is evident when comparing the *in vitro* and *in silico CS3* results. Moreover, the high signal intensity of the regions closer to the excitation coils are so large that they make the contribution from smaller signals insignificant in the inverse problem solution process, reducing the amount of high quality information.

Analyzing the *CV* values presented in the results section is possible to observe that when additional excitation and pick-up coils are active, the spatial sensitivity homogeneity increases. Furthermore, when pick-up coils are detecting the magnetic materials response from an another sensor's excitation coil magnetizing field (i.e., the pick-up coil detecting without the influence of their own excitation coils), their signal are less dependent of the material's radial position than when both pick-up and excitation coils from the same sensor are active together. This is confirmed by the *CV* lower values for *CS3* and *CS4* in comparison to *CS1* and *CS2*, for the fixed method. In addition, even the condition number $\boldsymbol{k}$ indicating that inverse problem solution is more stable for *CS1* and *CS2* for the fixed method, this does not guarantee a higher reconstruction performance, which is also strongly dependent of the *CV* value. The $\boldsymbol{k}$ values indicated that *CS3* and *CS4* are susceptible to a high amplification of perturbations (fixed method), but they

also carry a high amount of information that will increase convergence of the reconstruction to the nominal distribution, when in favorable experimental conditions. Note that the main reason of the low quality reconstruction of the *CS1*, *CS2*, and *CS4* setups is the low number of signals acquired.

In regards to the translated method, *CS3* and *CS4* showed better results than the fixed method. The improvement in sensitivity map homogeneity happens because the pick-up coils are closer to the materials during the translations (smaller FOV), increasing their sensitivity in the FOV. In this way, low intensity signals that were made insignificant by higher intensity signals in the fixed method, become more significant in the translated method. However, as before, the increased sensitivity (added by the new set of information of the closer pick-up coils translated) brings more instability to the inverse problem solution, mainly because of the high dependence of the magnetic material radial position. This fact is evident when analyzing the $\boldsymbol{k}$ values found for the translated method, which increased for the *CS3* and *CS4* when compared to the fixed method.

In this way, our results showed that the translated method presented the best performance for tomographic reconstructions of magnetic materials distributions. In special, the translated *CS3* setup showed the best combination of X_{diff} and *CC* values. In addition, the main issues found when using the ACB8 associated with the methods (fixed and translated) and setups (*CS1*, *CS2*, *CS3*, and *CS4*) studied here, are the high dependence of the magnetic material radial position in the FOV, and a low signal intensity in the center of the FOV, as expected. To improve the system's performance, one can increase the sensitivity map homogeneity, increasing the magnetic field amplitudes only in the FOV's center, and the number of excitation and pick-up coils, which would add more information to the problem. Therefore, future works can rotate the entire system and perform new sets of signal acquisition to "create" more sensors in intermediary positions, and also add large excitation coils parallel to the system's plane (magnetic field orthogonally oriented to the FOV). The first improvement can bring more information to the problem, while the second can improve the sensitivity map homogeneity. It is important to mention that when adding these excitation coils parallel to the sensor plane, is of paramount of importance to build them with an inner radius that allow the phantoms, or animals, cross the system's FOV to perform several tomographic slices, and consequently a volumetric reconstruction. Still, other works suggests to modulate the excitation coils current to increase the FOV homogeneity and the amount of information in the problem, and also optimize the activation sequence of the coils to avoid low quality information signals (23, 25, 27, 41).

Here, we presented a new ACB system setup that enabled the quantitative tomographic imaging of magnetic micro particles distributions. The results found here show the ACB8 potential to be future employed as a tool for quantitative tomographic imaging of organs and small animals. The ACB8 system presented a lower spatial resolution and quantification efficiency when compared to the standard techniques, but also presents advantages as the low cost, high versatility, and portability. We believe that with some instrumental improvements, it is possible to improve the results found here, increasing the system's spatial resolution and quantification power. Furthermore, the inverse problem details discussed here, as the sensitivity map homogeneity, coefficient of variation, and condition number impacts on the ACB inverse problem solution can bring light on future works, and lead to a better understanding of the ACB system inverse problem and new strategies to find better inverse solutions.

References

1. Dobson J. Magnetic micro-and nano-particle-based targeting for drug and gene delivery. 2006.
2. De Luca M, Aiuti A, Cossu G, Parmar M, Pellegrini G, Robey PGJNCB. Advances in stem cell research and therapeutic development. 2019;21(7):801-11.
3. Comanescu CJC. Magnetic Nanoparticles: Current Advances in Nanomedicine, Drug Delivery and MRI. 2022;4(3):872-930.
4. Khizar S, Ahmad NM, Zine N, Jaffrezic-Renault N, Errachid-el-salhi A, Elaissari AJAANM. Magnetic nanoparticles: From synthesis to theranostic applications. 2021;4(5):4284-306.
5. Kiaie N, Emami SH, Rabbani S, Aghdam RM, Tafti HAJAoBE. Targeted and controlled drug delivery to a rat model of heart failure through a magnetic nanocomposite. 2020;48(2):709-21.
6. Sommer WH, Sourbron S, Huppertz A, Ingrisch M, Reiser MF, Zech CJJAi. Contrast agents as a biological marker in magnetic resonance imaging of the liver: conventional and new approaches. 2012;37(2):164-79.
7. Bruno F, Granata V, Cobianchi Bellisari F, Sgalambro F, Tommasino E, Palumbo P, et al. Advanced Magnetic Resonance Imaging (MRI) Techniques: Technical Principles and Applications in Nanomedicine. 2022;14(7):1626.
8. Zhou Z, Yang L, Gao J, Chen XJAM. Structure–relaxivity relationships of magnetic nanoparticles for magnetic resonance imaging. 2019;31(8):1804567.
9. Weizenecker J, Gleich B, Rahmer J, Dahnke H, Borgert JJPiM, Biology. Three-dimensional real-time in vivo magnetic particle imaging. 2009;54(5):L1.
10. Ficko BW, Nadar PM, Hoopes PJ, Diamond SGJPiM, Biology. Development of a magnetic nanoparticle susceptibility magnitude imaging array. 2014;59(4):1047.
11. Coene A, Crevecoeur G, Dupre LJItom. Adaptive control of excitation coil arrays for targeted magnetic nanoparticle reconstruction using magnetorelaxometry. 2012;48(11):2842-5.
12. Crevecoeur G, Baumgarten D, Steinhoff U, Haueisen J, Trahms L, Dupré LJIToM. Advancements in magnetic nanoparticle reconstruction using sequential activation of excitation coil arrays using magnetorelaxometry. 2012;48(4):1313-6.
13. Maniam S, Szklaruk JJWjor. Magnetic resonance imaging: Review of imaging techniques and overview of liver imaging. 2010;2(8):309.
14. Prospero AG, Buranello LP, Fernandes CA, Dos Santos LD, Soares G, C Rossini B, et al. Corona protein impacts on alternating current biosusceptometry signal and circulation times of differently coated MnFe2O4 nanoparticles. 2021;16(24):2189-206.
15. Quini CC, Matos JF, Próspero AG, Calabresi MFF, Zufelato N, Bakuzis AF, et al. Renal perfusion evaluation by alternating current biosusceptometry of magnetic nanoparticles. 2015;380:2-6.
16. Calabresi M, Quini C, Matos J, Moretto G, Americo M, Graça J, et al. Alternate current biosusceptometry for the assessment of gastric motility after proximal gastrectomy in rats: a feasibility study. 2015;27(11):1613-20.
17. Corá LA, Américo MF, Oliveira RB, Baffa O, Moraes R, Romeiro FG, et al. Disintegration of magnetic tablets in human stomach evaluated by alternate current Biosusceptometry. 2003;56(3):413-20.
18. Prospero AG, Fidelis-de-Oliveira P, Soares GA, Miranda MF, Pinto LA, Dos Santos DC, et al. AC biosusceptometry and magnetic nanoparticles to assess doxorubicin-induced kidney injury in rats. 2020;15(05):511-25.
19. Corá L, Andreis U, Romeiro FG, Américo M, Oliveira RBd, Baffa O, et al. Magnetic images of the disintegration process of tablets in the human stomach by ac biosusceptometry. 2005;50(23):5523.

20. Soares GA, Prospero AG, Calabresi MF, Rodrigues DS, Simoes LG, Quini CC, et al. Multichannel AC Biosusceptometry system to map biodistribution and assess the pharmacokinetic profile of magnetic nanoparticles by imaging. 2019;18(3):456-62.
21. Biasotti GGdA, Próspero AG, Alvarez MDT, Liebl M, Pinto LA, Soares GA, et al. 2D Quantitative Imaging of Magnetic Nanoparticles by an AC Biosusceptometry Based Scanning Approach and Inverse Problem. 2021;21(21):7063.
22. Soares G, Pinto L, Liebl M, Biasotti G, Prospero A, Stoppa E, et al. Quantitative imaging of magnetic nanoparticles in an unshielded environment using a large AC susceptibility array. 2022.
23. Baumgarten D, Braune F, Supriyanto E, Haueisen JJJoM, Materials M. Plane-wise sensitivity based inhomogeneous excitation fields for magnetorelaxometry imaging of magnetic nanoparticles. 2015;380:255-60.
24. Schier P, Coene A, Jaufenthaler A, Baumgarten DJPiM, Biology. Evaluating selection criteria for optimized excitation coils in magnetorelaxometry imaging. 2021;66(23):235001.
25. Liebl M, Steinhoff U, Wiekhorst F, Haueisen J, Trahms LJPiM, Biology. Quantitative imaging of magnetic nanoparticles by magnetorelaxometry with multiple excitation coils. 2014;59(21):6607.
26. Hanson JD, Hirshman SPJPoP. Compact expressions for the Biot–Savart fields of a filamentary segment. 2002;9(10):4410-2.
27. Schier P, Liebl M, Steinhoff U, Handler M, Wiekhorst F, Baumgarten DJJoMI, et al. Optimizing excitation coil currents for advanced magnetorelaxometry imaging. 2020;62(2):238-52.
28. Jaufenthaler A, Schier P, Middelmann T, Liebl M, Wiekhorst F, Baumgarten DJS. Quantitative 2D magnetorelaxometry imaging of magnetic nanoparticles using optically pumped magnetometers. 2020;20(3):753.
29. Coene A, Crevecoeur G, Liebl M, Wiekhorst F, Dupré L, Steinhoff UJJoAP. Uncertainty of reconstructions of spatially distributed magnetic nanoparticles under realistic noise conditions. 2014;115(17):17B509.
30. Mukaka MMJMmj. A guide to appropriate use of correlation coefficient in medical research. 2012;24(3):69-71.
31. Soares GA, Faria JV, Pinto LA, Prospero AG, Pereira GM, Stoppa EG, et al. Long-Term Clearance and Biodistribution of Magnetic Nanoparticles Assessed by AC Biosusceptometry. 2022;15(6):2121.
32. Branquinho LC, Carrião MS, Costa AS, Zufelato N, Sousa MH, Miotto R, et al. Effect of magnetic dipolar interactions on nanoparticle heating efficiency: Implications for cancer hyperthermia. 2013;3(1):1-11.
33. Thiesen B, Jordan AJIjoh. Clinical applications of magnetic nanoparticles for hyperthermia. 2008;24(6):467-74.
34. Wiekhorst F, Steinhoff U, Eberbeck D, Trahms LJPr. Magnetorelaxometry assisting biomedical applications of magnetic nanoparticles. 2012;29(5):1189-202.
35. Ficko BW, Giacometti P, Diamond SGJJom, materials m. Nonlinear susceptibility magnitude imaging of magnetic nanoparticles. 2015;378:267-77.
36. Qiao R, Yang C, Gao MJJoMC. Superparamagnetic iron oxide nanoparticles: from preparations to in vivo MRI applications. 2009;19(35):6274-93.
37. Saritas EU, Goodwill PW, Croft LR, Konkle JJ, Lu K, Zheng B, et al. Magnetic particle imaging (MPI) for NMR and MRI researchers. 2013;229:116-26.
38. Corá LA, Romeiro FG, Paixao FC, Américo MF, Oliveira RB, Baffa O, et al. Enteric coated magnetic HPMC capsules evaluated in human gastrointestinal tract by AC biosusceptometry. 2006;23(8):1809-16.
39. Baffa O, Oliveira R, Arruda Miranda J, Troncon LJM, Engineering B, Computing. Analysis and development of AC biosusceptometer for orocaecal transit time measurements. 1995;33(3):353-7.

40. Quini CC, Américo MF, Corá LA, Calabresi MF, Alvarez M, Oliveira RB, et al. Employment of a noninvasive magnetic method for evaluation of gastrointestinal transit in rats. 2012;6(1):1-6.
41. Coene A, Leliaert J, Dupré L, Crevecoeur GJMP. Quantitative model selection for enhanced magnetic nanoparticle imaging in magnetorelaxometry. 2015;42(12):6853-62.